PHYSICAL REVIEW B **100**, 245208 (2019)

Dynamic defect as nonradiative recombination center in semiconductors

Junhyeok Bang,[1,4,*] Sheng Meng,[2] and S. B. Zhang[3,*]
[1]*Spin Engineering Physics Team, Korea Basic Science Institute, Daejeon 305-806, Republic of Korea*
[2]*Beijing National Laboratory for Condensed Matter Physics and Institute of Physics, Chinese Academy of Sciences, Beijing 100190, People's Republic of China*
[3]*Department of Physics, Applied Physics & Astronomy, Rensselaer Polytechnic Institute, Troy, New York 12180, USA*
[4]*Department of Physics, Chungbuk National University, Cheongju 28644, Republic of Korea*

(Received 30 May 2018; revised manuscript received 12 December 2019; published 30 December 2019)

We present a theory of nonradiative recombination (NRR) with an emphasis on the so far little-explored dynamic effect in the process. We show that it can significantly enhance the NRR rate over that of a static midgap level as suggested by the Shockley-Read-Hall theory, whereby offering an alternative explanation to the long-lasting discrepancy between theory and experiment for semiconductors. As an illustration, we show that dynamic NRR can take place at the *DX* center in Si-doped GaAs which, combined with a modified *ABC* model at high carrier-density limit, makes it possible to verify the theory directly by experiment.

DOI: 10.1103/PhysRevB.100.245208

I. INTRODUCTION

Nonradiative recombination (NRR) is an excited-state phenomenon, which manifests itself in various processes important to device applications such as suppressed luminescence, reduced carrier lifetime and density, creation of defects, and enhanced ion diffusion [1,2]. Traditionally, NRR has been extensively studied in the context of semiconductor physics and microelectronics. In recent years, it is also widely discussed in various cross-discipline renewable energy applications pertaining to light harvesting and related phenomena [3,4].

Excited carriers can undergo NRR by a defect level inside the band gap, as shown in Fig. 1(a), which is also termed the Shockley-Read-Hall (SRH) recombination [5,6]. To complete a cycle of NRR requires the capture of both an electron and a hole. As such, the slower capture process between the two determines the overall recombination rate. Because the capture rate exponentially decreases with the level position with respect to the band edges [7–9], the SRH theory states that, as a compromise, an active NRR center should have a midgap defect level. For over a half century, this SRH theory has been widely accepted for defect-induced NRR processes, as well as served as the guiding principles to identify key defects that hinder the performance of various optoelectronic devices.

While the SRH theory appears to explain experimental observations at least qualitatively [10–12], recent first-principles calculations showed that in a number of cases the theory could severely underestimate the recombination rates, e.g., the SRH parameter A (estimated from experiments) is on the order of $10^7\ \mathrm{s}^{-1}$ for InGaN alloys with a band gap around 3.0 eV [12], while the theoretical estimate $<10^3\ \mathrm{s}^{-1}$ is significantly smaller [7–9,13,14]. In essence, NRR is not a static process because the excited carriers involved are fast-evolving species, which shed their energies to the surroundings of the defect at a comparable rate. However, the SRH model assumed implicitly the adiabatic approximation, i.e., static levels for the defects, as at the time of their studies, a nonadiabatic theory was still being made [15]. Given the discrepancy, one may question the foundation of the SRH theory, namely, the adiabatic approximation. We note that the energy levels can shift considerably as a result of carrier capture and concomitant atomic reconfigurations, as shown in Fig. 1(b) for a dynamic defect. In the past, it was impossible to theoretically study such an effect, until recently when the recent development of time-dependent density-functional theory (TDDFT)–molecular dynamics (MD) made such a study a real possibility.

In this paper, we expand the NRR theory by including explicitly dynamic effects at defects. We show that the NRR rate at a dynamic defect can be orders of magnitude larger than that of a fixed midgap level as suggested by the SRH theory. When taking into account the dynamic effects, the rate equation for the NRR also deviates from the linear dependence on the carrier density n in the high-density limit. As a result, the widely accepted *ABC* rate equation is modified. Using TDDFT-MD, we show that Si-on-Ga donor in GaAs could be an example of the dynamic NRR center. Normally, this shallow donor is not a dynamic defect but when the condition is met such as by applying pressure, the donor becomes a deep-level defect known as the *DX* center by capturing an electron. The doubly occupied deep level is near the valence-band maximum (VBM), which can easily accept a hole so the defect returns to its original state. Since the onset of the *DX* behavior can be experimentally controlled, it is possible to measure directly such a dynamic NRR.

This paper is organized as follows. The theoretical formulation of recombination at a dynamic shallow level is described in Sec. II. In Sec. III we present technical details of the computational methods. In Sec. IV, we present the results for *DX* center in GaAs. Section V concludes the paper.

---

[*] Corresponding authors: jbang@cbnu.ac.kr; zhangs9@rpi.edu

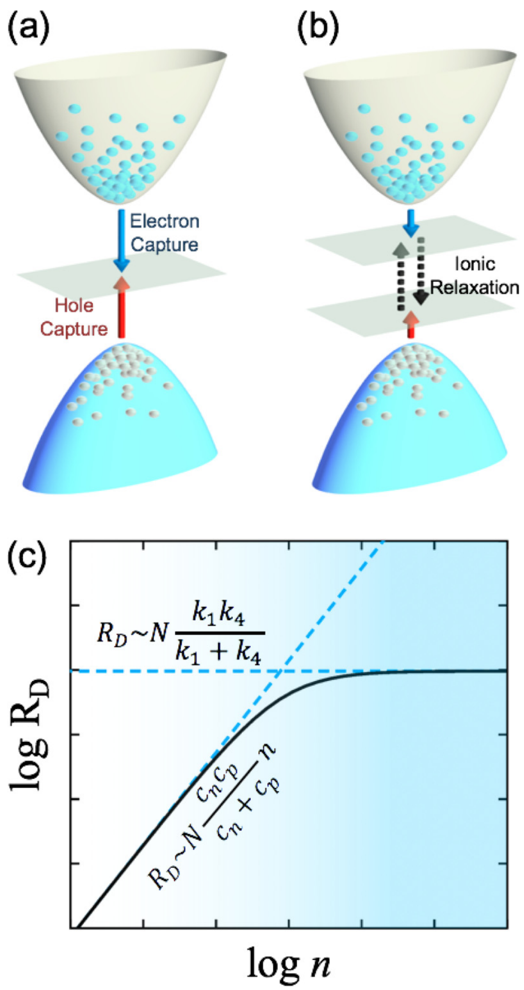

FIG. 1. Carrier recombination processes: (a) SRH recombination where excited electrons and holes are recombined at a static midgap level. (b) Dynamic NRR where capture of a carrier could lead concomitant ionic relaxation and level change. Solid blue and red arrows stand for electron and hole captures, respectively, dotted black arrow stands for ionic relaxation, and gray planes stand for defect levels inside the band gap. (c) Log-log plot of dynamic NRR rate versus carrier density, showing a linear increase with n in the low-density limit (similar to SRH), which turns into a constant in the high-density limit.

II. THEORETICAL FORMULATION OF RECOMBINATION AT A DYNAMIC SHALLOW LEVEL

As discussed above, the capture of a carrier at the defect can lead to a large ionic relaxation due to strong electron-phonon coupling. For such a process, the NRR rate is derived as

$$R_D = N \frac{n c_n p c_p k_1 k_2}{n c_n p c_p k_1 + n c_n p c_p k_2 + n c_n k_1 k_2 + p c_p k_1 k_2}, \quad (1)$$

where N is the concentration of the dynamic defects, c_n and c_p are, respectively, the electron and hole capture rates, k_1 and k_2 are the rates of the concomitant ionic relaxations, and all rates are given in unit volume (see Appendix A). Under thermal equilibrium, k_i is given by the Boltzmann factor: $k_i = f \exp[-E_i/k_B T]$, where f is the vibration frequency, E_i is the energy barrier, and k_B and T are the Boltzmann constant and temperature. Assume $n \sim p$; in the low carrier density limit, i.e., when (nc_n and pc_p)$\ll$ (k_1 and k_2), Eq. (1) is linear with n, i.e.,$R_D \sim N \frac{c_n c_p}{c_n + c_p} n$, which agrees with that of SRH. In the high carrier-density limits, i.e., when (nc_n and pc_p)$\gg$(k_1 and k_2), however, Eq. (1) is noticeably different from that of SRH, as it becomes independent of n, i.e., $R_D \sim N \frac{k_1 k_2}{k_1 + k_2}$ as can be seen in Fig. 1(c). This is a hallmark difference, which should clearly show up in experiments.

An important type of dynamic NRR occurs when the concomitant ionic relaxation leads to dynamic shallow levels (DSLs), which are shallow at both band edges: for example, the capture of an electron at a shallow level from the conduction-band minimum (CBM) leads to a large ionic relaxation to result in a shallow level measured from the VBM to capture a hole easily. Due to the shallowness, both c_n and c_p are considerably larger than the capture rate by a static and deep-level defect, c_n^d and c_p^d. From Eq. (1), one deduces the condition

$$\min[k_1, k_2] \geqslant 2n \min\left[c_n^d, c_p^d\right], \quad (2)$$

at which the DSL defect will surpass the "nondynamic" SRH defect (see Appendix B). Note that, while our discussion here will focus on the DSL, any negative-U center [16] with reasonably shallow dynamic levels may satisfy Eq. (2), whereby acting as an active NRR center. Under the working condition of an optoelectronic device, n is typically $< 10^{19}\ \mathrm{cm}^{-3}$. Because the quantity $\min[c_n^d,\ c_p^d]$ is mainly determined by the position of the defect level and is maximized at the midgap level, the controlling factor for SRH is the band gap of the system. For instances, for GaAs the midgap position is about 0.7 eV away from band edges and the estimated c_n^d and c_p^d are in the range of 10^{-8}–$10^{-10}\ \mathrm{cm}^3/\mathrm{s}$ [8]. According to Eq. (2), $\min[k_1, k_2]$ should be larger than $10^{10}\ \mathrm{s}^{-1}$. For GaN, on the other hand, the midgap position is about 1.7 eV away from band edges and the estimated c_n^d and c_p^d are smaller than $10^{-14}\ \mathrm{cm}^3/\mathrm{s}$ [8,9]. As such, $\min[k_1, k_2]$ should only be larger than $10^4\ \mathrm{s}^{-1}$.

III. COMPUTATIONAL METHODOLOGY

A. Total energy calculation

The rates of the carrier capture and the concomitant ionic relaxation were calculated based on the density-functional theory (DFT) and the time-dependent density-functional theory (TDDFT). We used the norm-conserving Troullier-Martins pseudopotentials [17] and local density-functional approximation (LDA) for the exchange-correlation potential [18], as implemented in the SIESTA program [19]. The Ga $3d$ orbitals were included in the valence shell. A local basis set with double-ζ polarized orbitals was employed. The real-space grid was equivalent to a plane-wave cutoff energy of 150 Ry. We used a periodic supercell containing 216 atoms to model GaAs. Γ-point sampling was used in the Brillouin-zone integration. Atomic structures were fully relaxed until the residual forces were less than 0.01 eV/Å. The nudged elastic band method [20], which was implemented in the ASE package [21], was used to find the energy barrier along the transition pathway from d to DX.

B. Real-time TDDFT-MD

For a given initial electronic wave function $\{\varphi_i(r, t = 0)\}$ and atomic configuration (positions $\{R_j\}$ and velocities $\{\dot{R}_j\}$), we solve the time-dependent Kohn-Sham equation [22], i.e.,

$$i\hbar\frac{\partial\varphi_i(r,t)}{\partial t} = \left(-\frac{\hbar^2}{2m}\nabla_r^2 + V_s[\rho, \{R_j\}](r,t)\right)\varphi_i(r,t) \tag{3}$$

for electron dynamics, and the Newton equation for lattice dynamics based on TDDFT [22] and molecular dynamics. Using the two equations, electron and lattice-coupled dynamics, such as carrier relaxation and carrier capture by carrier-carrier and carrier-lattice scatterings, is simulated in real time. This TDDFT-MD formalism is implemented in the code developed based on the SIESTA program [19,23,24]. The DFT parameters were the same as those in time-independent calculations. In the dynamic calculations, we used a time step of 25 attoseconds and the Ehrenfest approximation for ion motion. To prepare the initial atomic configuration, we performed electron ground-state MD simulations to extract equilibrated atomic coordinates and velocities at a lattice temperature of 300 K. For the initial electronic wave functions, we used the occupation-constrained DFT calculation [25], which performs the self-consistent-field calculation with constrained electron occupation on each energy level. This method has been widely used in previous works [26,27].

IV. RESULTS

From the discussions in Sec. II, *DX* centers in semiconductors with desired DSL [28–34] are a good candidate to test the dynamic NRR theory. The *AX* centers [35,36], which act as a mirror image of the *DX* centers, are another candidate. Here, we consider Si in GaAs for it, which has been widely studied in the past [28–30]. A charge-neutral Si atom normally would substitute a Ga atom on the lattice site with the T_d symmetry, as shown in Fig. 2(a). This substitutional Si will be denoted as *d*. By capturing an electron from the Fermi level and breaking one of its four Si–As bonds, the Si atom can undergo a large atomic displacement to a nearest interstitial site with a C_{3v} symmetry, as shown in Fig. 2(b). This "interstitial-vacancy" pair is known as the *DX* center. While *d* has a shallow donor level [37], the *DX* has a deep *DX* level near the VBM originated from the Si dangling-bond state [28–30]. While bond breaking usually increases energy, here the lowering of the doubly occupied level from near the CBM to near the VBM compensates for the energy increase. Hence, the DX^- is stabilized. Experiments showed that the DX^- center becomes stable under a hydrostatic pressure of 20 kbar or higher or inside an $\mathrm{Al}_x\mathrm{Ga}_{1-x}\mathrm{As}$ alloy with $x > 22\%$ [31].

The relative stability between d^- and DX^- depends sensitively on the applied pressure [31–33], which is also reproduced by our density-functional theory calculations: without pressure, d^- is more stable by 0.58 eV; at 1% compressive strain (CS), the energy difference is reduced to 0.09 eV; at 2% CS, DX^- becomes more stable by 0.13 eV; and at 3% CS, DX^- is more stable by another 0.18 eV, as depicted in Fig. 2(c). Along with the change in the relative stability, the transition energy barrier from d^- to DX^- is also reduced from 0.73 eV at zero pressure to 0.05 eV at 3% CS. Assuming a vibration frequency of 8 THz for GaAs [38], one can estimate the transition rate using the Boltzmann equation. At room temperature, it is 4.3, 1.6×10^8, 2.5×10^{11}, and $1.2 \times 10^{12}\ \mathrm{s}^{-1}$ for 0, 1, 2, and 3% CS, respectively. It is important to note that the *DX* centers become active NRR centers [namely, satisfying Eq. (2)], only when the sample is under a hydrostatic pressure.

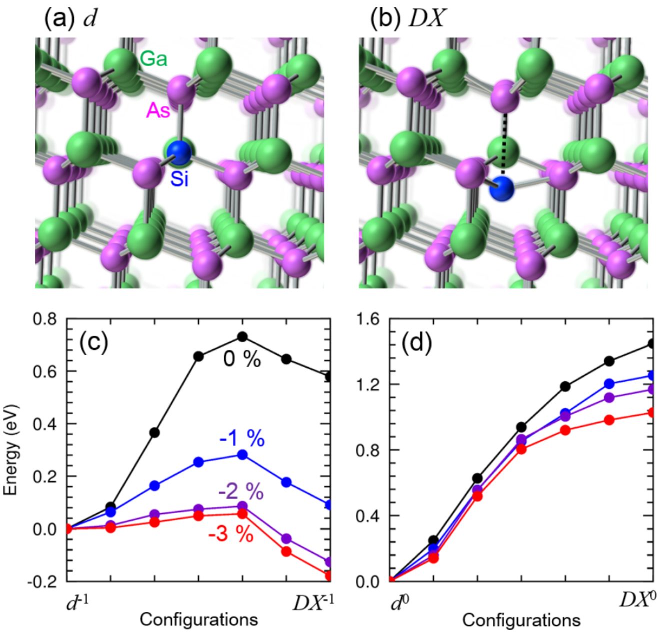

FIG. 2. Atomic structures of (a) *d* and (b) *DX*. Configurational energy diagrams for (c) (−1) and (d) (0) charge states. Black, blue, violet, and red lines stand for 0, 1, 2, and 3% compressions, respectively.

The doubly occupied DX^- level can greatly enhance the ability of the center to capture a hole from the VBM. However, after the hole capture, the resulting DX^0 will no longer be stable and it will spontaneously return to d^0, as can be seen in Fig. 2(d). It turns out that such a hole capture process, involving considerable atomic restructuring and relaxation, is an ultrafast nonadiabatic process for which the Born-Oppenheimer approximation used in the DFT calculations is highly questionable. In this study, we perform instead nonadiabatically coupled TDDFT and MD simulations at 300 K.

To mimic the initial excited state of the hole capture, we took electrons from the VBM and placed them in *DX* levels. In the TDDFT calculations, the dynamics of the carriers is represented by changes in the wave functions. As time develops, the initial state $|\varphi(t = 0)\rangle = |i\rangle$ evolves into a superposition of various states, i.e., $|\varphi(t)\rangle = \sum_j a_j(t)|j\rangle$. In the current case, there is only one state, i.e., $|DX\rangle$, initially with its energy level inside the band gap. At a later time *t*, it evolves into $|\varphi(t)\rangle = a_{DX}(t)|DX\rangle + a_{VBM}(t)|VBM\rangle$, where $|VBM\rangle$ is the state at the valence-band maximum. It represents an electron transfer from $|DX\rangle$ to the $|VBM\rangle$, and we can extract the capture rate from coefficient $a_{DX}(t)$. In our supercell calculation, the calculated rate *W*, which is the inverse of the hole capture time in the TDDFT-MD simulation, is given on condition that the *DX* center exists with a density $N_{DX} = 1/V$ [*V* is the volume of the supercell]. The capture rate c_p by a *DX* defect per unit volume is given by $c_p = W/N_{DX} = WV$.

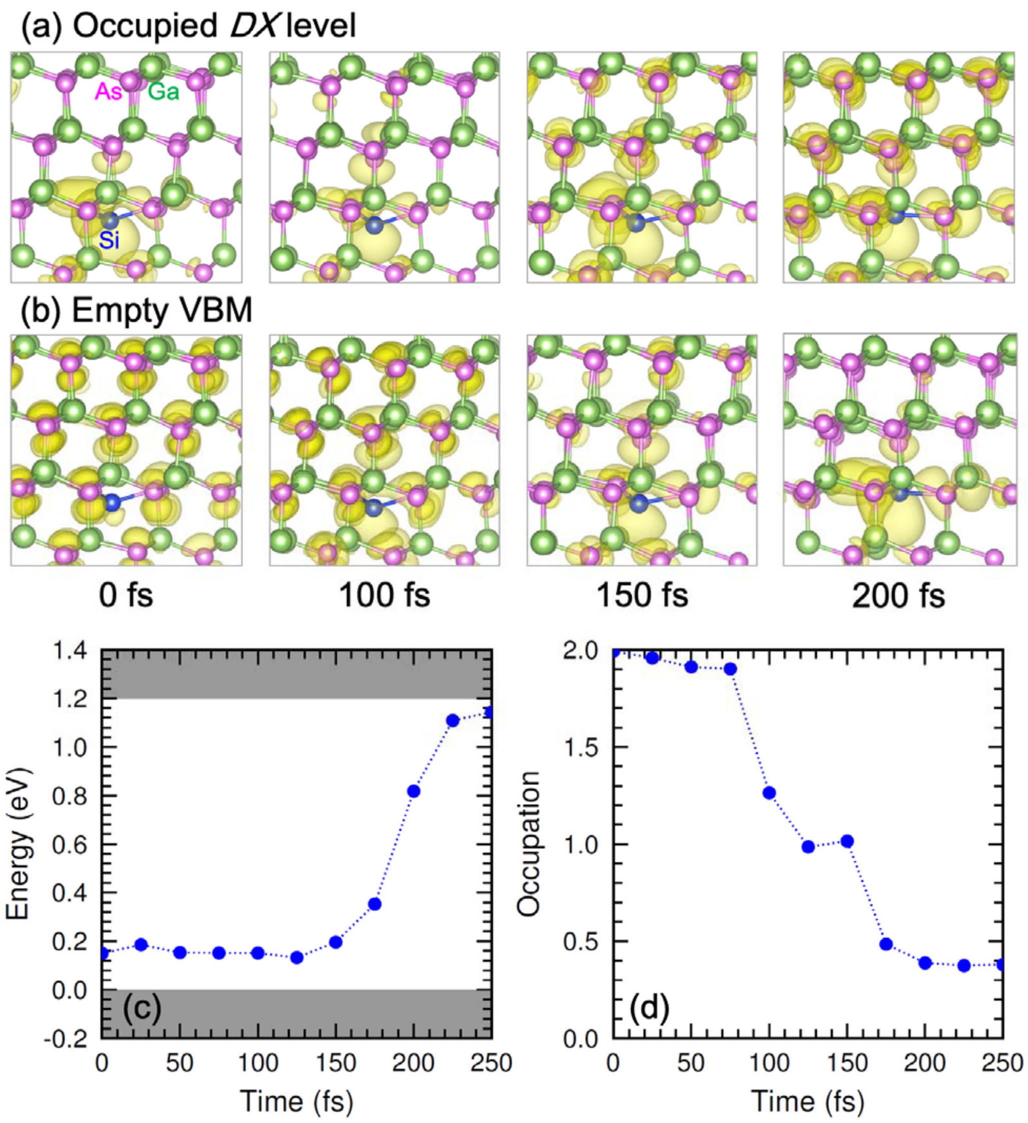

FIG. 3. Dynamics of hole capture. Snapshots of time evolution of charge densities for (a) doubly occupied *DX* and (b) empty VBM states. Time evolution of (c) adiabatic *DX* level and (d) the corresponding electron occupancy in the TDDFT-MD simulation.

As an initial conditioning of the simulation using a supercell, we place two electrons at the *DX* level and two holes at the VBM, which will recombine with the electrons. While we have considered CS from 0 to 3%, the results are qualitatively the same, so only the results for 2% CS will be discussed here. Figures 3(a) and 3(b) show how the charge densities of the initially occupied *DX* level and the initially empty VBM level evolve with time. Note that these states will change their characters during the simulation. Initially, the *DX* state is localized near the Si atom, while the VBM state is delocalized. As time goes on, the *DX* state becomes delocalized and approaches the initial VBM state. Conversely, the VBM state becomes localized and approaches the initial *DX* state. Hence, Figs. 3(a) and 3(b) reveals that, in the final stage of the simulation, the VBM state is occupied whereas the *DX* state is empty. In other words, holes at the VBM have been captured by the *DX* centers.

To quantify the hole capture dynamics, we calculate the electron occupation of the *DX* level by projecting the time-evolved wave function onto that of an adiabatic *DX* level, which is an eigenstate of the Hamiltonian at a given time [39,40]. Figure 3(c) shows the time evolution of the adiabatic *DX* level: initially, it hovers around 0.15 eV above the VBM. At about 150 fs, this level starts to increase quickly toward the CBM, as the *DX* returns to *d*. Figure 3(d) shows the occupation of the defect level, which is initially at 2. At about 75 fs, a steep drop takes place, followed by another steep drop at about 150 fs. The smallest occupation number is 0.38 (or 19%), which is reached at about 200 fs. A fractional occupation in the TDDFT within the Ehrenfest approximation may be interpreted as a superposition of two separate processes [41,42]: one captures one hole while the other captures two holes, respectively. The results clearly show that the hole capture occurs within 200 fs. Note that the radiative process is also one possible channel of the hole capture, but it also removes the excited carriers with infrared light emission, not the band-edge transition.

To check whether the above TDDFT-MD results are statistically meaningful, we also performed seven other simulations at 300 K with different initial atomic positions and velocities. Qualitatively the same results were obtained: i.e., ultrafast hole captures within 150–250 fs. As a comparison, we also performed TDDFT-MD simulations for hole capture by d^-, but found nothing throughout the simulation. This can be understood because the energy of the shallow-donor level is too far away from the VBM.

The LDA exchange-correlation potential underestimates band gap, and it may affect the results. In the LDA calculations, the band gap of GaAs (E_g) is 0.93 eV (cf. 1.43 eV in experiments) and the DX level (ε_{DX}) is 0.2 eV measured from VBM (without strain). For comparison, we also preformed the Heyd-Scuseria-Ernzerhof (HSE) hybrid functional calculations [43] using the VASP program [44]. Here, the core electrons are described by the projector-augmented wave method [45] and we use a mixing parameter $\alpha = 0.35$ and screening parameter $\mu = 0.2\,\text{Å}^{-1}$, which are taken from Ref. [46]. The energy cutoff for the plane-wave basis is set to 300 eV. We use other parameters similar to the LDA calculation. In the HSE calculation, the band gap is 1.53 eV and ε_{DX} is 0.31 eV from the VBM. To examine the effect due to a change in the DX level, we choose to apply a strain to alter the DX level position (calculated within LDA). Without the strain, ε_{DX} is 0.2 eV above the VBM; with a 4% compressive strain, it is 0.1 eV above. Their difference (0.1 eV) is similar to the difference in the DX level between LDA (0.2 eV) and HSE (0.31 eV). While strain can also alter the carrier capture rate, we expect that such an effect is secondary. Using the TDDFT calculation, we found that, without the strain, the hole capture rate c_p is $1.3 \times 10^{-8}\,\text{cm}^3/\text{s}$. With a 4% compressive strain, it is $3.2 \times 10^{-8}\,\text{cm}^3/\text{s}$. In other words, a 0.1-eV energy-level change can enhance the capture rate by a factor of 2 to 3. This change should not affect the qualitative discussion and the conclusion of the paper.

Note that hole capture changes the charge state of Si from (−1) to either (0) or (+1). However, neither DX^0 nor DX^+ is stable, as shown in Fig. 2(d). A structural transition from DX to d is therefore inevitable as can be seen in Figs. 3(a) and 3(b). If we compare the left panel at 0 fs and the right panel at 200 fs, the Si atom has moved up significantly towards the T_d site, and the adiabatic level moves toward CBM [see Fig. 3(c)]. The delay time for a significant change in the structure is only 75 fs from the initial drop in the electron occupation at 75 fs [see Fig. 3(d)]. These findings reinforce the notion that the hole capture in semiconductors can be highly nonadiabatic.

We can summarize the overall recombination process as follows. Step 1: the acceptance of an electron at d^0. It is known that the time is short, typically that for carrier thermalization (∼tens of femtoseconds) [47,48]; Step 2: the resulting d^- undergoes a structural transition to DX^- with an energy-level lowering to near the VBM in no more than a few picoseconds; Step 3: hole capture from the VBM quickly happens, so the DX^0 spontaneously returns back to d^0. Step 2 is an activated process, which depends on pressure, and it can hence be maximally controlled in experiment.

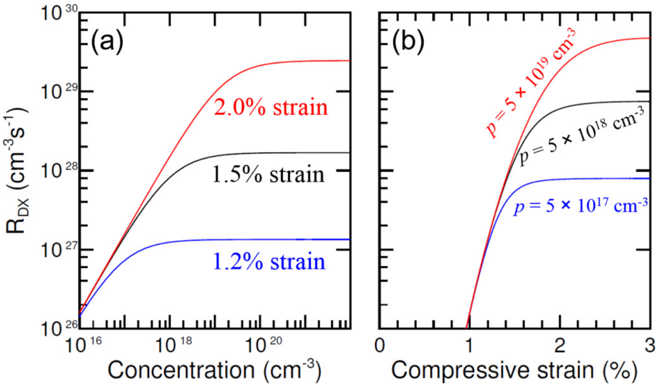

FIG. 4. Recombination rate R_{DX} of a DX center with respect to (a) hole concentration and (b) CS at $T = 300\,\text{K}$. In (a), blue, black, and red lines stand for 1.2, 1.5, and 2.0% CS, respectively. In (b), blue, black, and red lines stand for $p = 5 \times 10^{17}$, 5×10^{18}, and $5 \times 10^{19}\,\text{cm}^{-3}$, respectively.

To calculate the recombination rate, the first and last terms in the denominator in Eq. (1) can be neglected, as detailed in Appendix A. Therefore,

$$R_{DX} = N \frac{p c_p k_1}{p c_p + k_1}. \tag{4}$$

In a typical experiment [31], N is around $10^{18}\,\text{cm}^{-3}$, which will be used here and $c_p = 1.6 \times 10^{-8}\,\text{cm}^3/\text{s}$ has been determined by our calculation. The remaining parameter in Eq. (4) is k_1, which is an exponential function of the transition barrier E_1. We have interpolated the calculated E_1 as a function of CS using a cubic polynomial fitting. The resulting R_{DX} versus p and CS are shown in Figs. 4(a) and 4(b), respectively. The aforementioned transition of R_D in Fig. 1(c) is clearly observed for the DX center at a modest carrier density, typical for optoelectronic devices, as shown in Fig. 4(a). Figure 4(b) further shows that, as a function of CS, R_{DX} changes by orders of magnitude from far below the detection limit to readily detectable. This high sensitivity to pressure is a unique property of the DX-center-based NRRs, which should be checked out by experiment.

As a final remark, let us consider GaN, which is a wide-gap semiconductor. For midgap levels, $c_n^d \sim c_p^d$. As such, the SRH recombination rate is $R_{\rm SRH} \sim N_d \frac{c_n^d c_p^d}{c_n^d + c_p^d} n \sim \frac{1}{2} N_d c_n^d n = An$, where N_d is the mid-gap defect density. Note that here c_n^d and c_p^d are the capture rate by a static and deep-level defect. As such, they are much smaller than c_n and c_p of DSL. As a matter of fact, different first-principles calculations showed that c_n^d of GaN (band gap = 3.4 eV) should be $<10^{-14}\,\text{cm}^3/\text{s}$ [8,9,13,14]. From this value and a reasonable $N_d \sim 10^{17}\,\text{cm}^{-3}$, one obtains $A \sim 10^2\,\text{s}^{-1}$. However, the measured c_n (in the range of $10^{-8}\,\text{cm}^3/\text{s}$) and A (in the range of $10^7\,\text{s}^{-1}$) in photo- and electroluminescence experiments are much higher [12,49–53]. To account for the difference, a multilevel metastable-state-mediated NRR mechanism has been proposed [54]. Here, our results suggest that the dynamic effect could explain the discrepancy. In GaN, both DX centers and Frenkel pairs [55,56] may exist. As in GaAs, the DX centers in GaN may be experimentally controlled, so one can readily test the theory.

V. CONCLUSIONS

In summary, we complete the NRR theory to include both static and dynamic effects. Our central message here is that dynamic processes can be important for the NRR as well. We offer the DSL recombination at the *DX* centers as an unambiguous test of our theory, because the formation of the *DX* can be controlled experimentally by applying a hydrostatic pressure. Also different from most of the existing defect theories, here we offer a recombination process at the defect to be experimentally studied. Because the condition for a dynamic recombination can be more stringent than simply forming a static defect, our theory points to a different perspective in terms of designing low-cost materials for future microelectronics and optoelectronics.

ACKNOWLEDGMENTS

Work at Korea Basic Science Institute (KBSI) and Chungbuk National University was supported by Basic Science Research Program through the National Research Foundation of Korea (NRF) (Grant No. NRF-2018R1D1A1B07044564), National Research Council of Science & Technology (Grant No. CAP-18-05-KAERI), and KBSI Grant No. D39614. Work at Rensselaer Polytechnic Institute was supported by the US Department of Energy under Grant No. DE-SC0002623. Work at Chinese Academy of Sciences was supported by MOST (Grant No. 2016YFA0300902) and NSFC (Grant No. 11774396) We used the VESTA software to generate some of the figures [57].

APPENDIX A: RECOMBINATION RATE AT A DYNAMIC DEFECT

Figure 5 shows schematically the recombination processes at a dynamic defect, which will be used to derive Eq. (1). Given a process *A*, the rate ($\mathrm{P_A}$) would be

$$P_{\mathrm{EC}} = nc_n N[\mathrm{H^U}], \quad P_{\mathrm{EE}} = e_n N[\mathrm{H^O}],$$
$$P_{\mathrm{HC}} = pc_p N[\mathrm{L^O}], \quad P_{\mathrm{HE}} = e_p N[\mathrm{L^U}],$$
$$P_{K1} = k_1 N[\mathrm{H^O}], \quad P_{\overline{K}1} = \overline{k}_1 N[\mathrm{L^O}],$$
$$P_{K2} = k_2 N[\mathrm{L^U}], \quad P_{\overline{K}2} = \overline{k}_2 N[\mathrm{H^U}],$$

where n and p are the electron and hole carrier densities, c_n and c_p are the n/p capture rates by a dynamic level, e_n and e_p are the n/p emission rates, and k_i ($\overline{k}_i$) is the rate for structure transition in process Ki ($\overline{\mathrm{K}}$i) in Fig. 5. All rates are in unit of volume. N[X] is the density of defect X levels. In the derivation, we assume the n/p densities in the conduction and valence bands are small enough, so the occupation of the bands has no effect on the rates [5]. One can ignore the other small rate processes, i.e., electron capture to $\mathrm{L^U}$, electron emission from $\mathrm{L^O}$, hole capture to $\mathrm{H^O}$, and hole emission from $\mathrm{H^U}$. Under the steady-state condition, $\frac{dN[\mathrm{X}]}{dt} = 0$, so we arrive at

$$\frac{dN[\mathrm{H^U}]}{dt} = 0 = -nc_n N[\mathrm{H^U}] - \overline{k}_2 N[\mathrm{H^U}] + e_n N[\mathrm{H^O}] + k_2 N[\mathrm{L^U}], \tag{A1a}$$

$$\frac{dN[\mathrm{H^O}]}{dt} = 0 = -e_n N[\mathrm{H^O}] - k_1 N[\mathrm{H^O}] + nc_n N[\mathrm{H^U}] + \overline{k}_1 N[\mathrm{L^O}], \tag{A1b}$$

$$\frac{dN[\mathrm{L^U}]}{dt} = 0 = -e_p N[\mathrm{L^U}] - k_2 N[\mathrm{L^U}] + pc_p N[\mathrm{L^O}] + \overline{k}_2 N[\mathrm{H^U}], \tag{A1c}$$

$$\frac{dN[\mathrm{L^O}]}{dt} = 0 = -pc_p N[\mathrm{L^O}] - \overline{k}_1 N[\mathrm{L^O}] + e_p N[\mathrm{L^U}] + k_1 N[\mathrm{H^O}]. \tag{A1d}$$

Only three Eqs. (A1a)–(A1c) are independent, as the summation of them yields Eq. (A1d). In addition, conservation of the total number of defect states (defined as N) requires that

$$N = N[\mathrm{H^U}] + N[\mathrm{H^O}] + N[\mathrm{L^U}] + N[\mathrm{L^O}]. \tag{A1e}$$

By some detailed algebra, we obtain

$$\frac{N[\mathrm{H^U}]}{C[\mathrm{H^U}]} = \frac{N[\mathrm{H^O}]}{C[\mathrm{H^O}]} = \frac{N[\mathrm{L^U}]}{C[\mathrm{L^U}]} = \frac{N[\mathrm{L^O}]}{C[\mathrm{L^O}]}, \tag{A2}$$

where $C[\mathrm{H^U}] = e_n(\overline{k}_1 e_p + k_2 pc_p) + k_2(pc_p k_1 + e_n \overline{k}_1)$, $C[\mathrm{H^O}] = nc_n(k_2 pc_p + \overline{k}_1 e_p) + \overline{k}_1(e_p \overline{k}_2 + nc_n k_2)$, $C[\mathrm{L^U}] = pc_p(k_1 nc_n + \overline{k}_2 e_n) + \overline{k}_2(e_n \overline{k}_1 + pc_p k_1)$, and $C[\mathrm{L^O}] = e_p(\overline{k}_2 e_n + k_1 nc_n) + k_1(nc_n k_2 + e_p \overline{k}_2)$. From Eq. (A2), we derive

$$N[\mathrm{X}] = N \frac{C[\mathrm{X}]}{C[\mathrm{H^U}] + C[\mathrm{H^O}] + C[\mathrm{L^U}] + C[\mathrm{L^O}]}. \tag{A3}$$

Using Eq. (A3), the recombination rate R_D (per unit volume) under the steady-state condition is

$$R_D = N \frac{nc_n pc_p k_1 k_2 - e_n e_p \overline{k}_1 \overline{k}_2}{C[\mathrm{H^U}] + C[\mathrm{H^O}] + C[\mathrm{L^U}] + C[\mathrm{L^O}]}. \tag{A4}$$

For an active NRR center, the carrier capture (P_{EC} and P_{HC}) and concomitant ionic relaxation (P_{K1} and P_{K2}) must dominate over the carrier emission (P_{EE} and P_{HE}) as well as backward ionic relaxation ($P_{\overline{K}1}$ and $P_{\overline{K}2}$). Under such a condition, we can set in Eq. (A4) $e_n = e_p = 0$ (the carrier emission) and $\overline{k}_1 = \overline{k}_2 = 0$ (the backward ionic relaxation) to obtain Eq. (1).

In case of the *DX* center, because P_{EC} and P_{K2} are ultrafast processes (c_n and $k_2 \rightarrow \infty$), the first and last terms in the denominator of Eq. (1) can be neglected, which leads to Eq. (4).

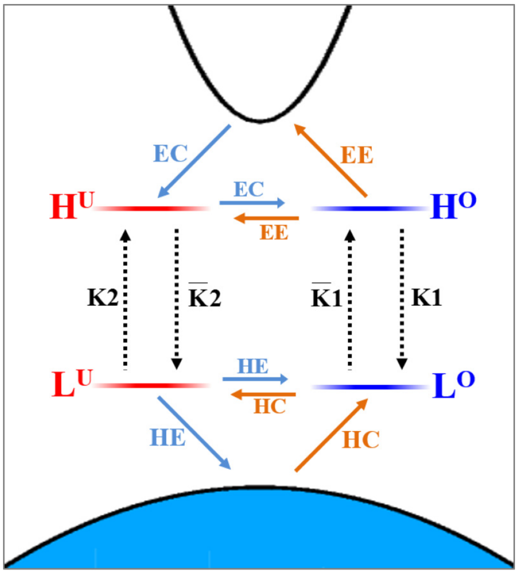

FIG. 5. Schematic diagram for processes in dynamic nonradiative recombination. Arrows EC (HC) and EE (HE) represent the electron (hole) capture and emission processes, respectively, whereas black dotted arrows Ki and $\overline{\mathrm{K}}$i are the concomitant ionic relaxation processes. The four horizontal lines represent the dynamic changes of an energy level during the recombination: they are the occupied (blue) high-energy level (H^{O}), unoccupied (red) high-energy level (H^{U}), occupied (blue) low-energy level (L^{O}), and unoccupied (red) low-energy level (L^{U}). Carrier capture and emission lead to changes among the charge states (horizontal path), while the concomitant ionic relaxations lead to changes between high and low-energy states (vertical path).

APPENDIX B: CONDITION AT WHICH DSL DOMINATES OVER SRH

The rate for SRH recombination is

$$R_{\mathrm{SRH}} = N_d \frac{nc_n^d pc_p^d}{nc_n^d + pc_p^d}, \tag{B1}$$

where c_n^d and c_p^d are, respectively, the rates for electron and hole captures by a deep-level defect. Here, we can also ignore the carrier emission processes. It happens that the math can be easier if we work with the inverse of R, such that $\frac{N}{R_D} = \frac{1}{nc_n} + \frac{1}{pc_p} + \frac{1}{k_1} + \frac{1}{k_2}$ for DSL and $\frac{N}{R_{\mathrm{SRH}}} = \frac{1}{nc_n^d} + \frac{1}{pc_p^d}$ for SRH. The condition that DSL is more efficient than SRH is

$$\frac{1}{k_1} + \frac{1}{k_2} \leqslant \frac{1}{nc_n^d} + \frac{1}{pc_p^d} - \left(\frac{1}{nc_n} + \frac{1}{pc_p}\right). \tag{B2}$$

Because c_n and c_p for DSL states are much larger than c_n^d and c_p^d for deep-level defects, one can ignore the last term on the right-hand side. Moreover, the left-hand side of Eq. (B2) satisfies the inequality $\frac{1}{k_1} + \frac{1}{k_2} \leqslant \frac{2}{\min[k_1,k_2]}$, whereas the right-hand side of Eq. (B2) satisfies the inequality $\frac{1}{n}\frac{1}{\min[c_n^d,c_p^d]} \leqslant \frac{1}{nc_n^d} + \frac{1}{pc_p^d}$ when $n = p$ is assumed. Here, $\min[A, B]$ is the smaller of A and B. This leads to

$$\min[k_1, k_2] \geqslant 2n \min[d_n, d_p].$$

When $k_1 \ll k_2$ or $k_1 \gg k_2$, the condition can be relaxed to $\min[k_1, k_2] \geqslant n \min[d_n, d_p]$. The above one is more stringent inequality, when $k_1 \sim k_2$.

---

[1] A. M. Stoneham, *Theory of Defects in Solids* (Oxford University Press, Oxford, 1975), Chap. 14.
[2] A. M. Stoneham, Rep. Prog. Phys. **44**, 1251 (1981).
[3] B. G. Mendis, D. Gachet, J. D. Major, and K. Durose, Phys. Rev. Lett. **115**, 218701 (2015).
[4] M. C. Heiber, C. Baumbach, V. Dyakonov, and C. Deibel, Phys. Rev. Lett. **114**, 136602 (2015).
[5] W. Shockley and W. T. Read, Phys. Rev. **87**, 835 (1952).
[6] R. N. Hall, Phys. Rev. **87**, 387 (1952).
[7] L. Shi and L.-W. Wang, Phys. Rev. Lett. **109**, 245501 (2012).
[8] L. Shi, K. Xu, and L.-W. Wang, Phys. Rev. B **91**, 205315 (2015).
[9] A. Alkauskas, Q. Yan, and C. G. Van de Walle, Phys. Rev. B **90**, 075202 (2014).
[10] C. H. Henry and D. V. Lang, Phys. Rev. B **15**, 989 (1977).
[11] M. A. Reshchikov and R. Y. Korotkov, Phys. Rev. B **64**, 115205 (2001).
[12] J. Piprek, Phys. Status Solidi A **207**, 2217 (2010).
[13] C. E. Dreyer, A. Alkauskas, J. L. Lyons, J. S. Speck, and C. G. Van de Walle, Appl. Phys. Lett. **108**, 141101 (2016).
[14] J.-X. Shen, D. Wickramaratne, C. E. Dreyer, A. Alkauskas, E. Young, J. S. Speck, and C. G. Van de Walle, Appl. Phys. Express **10**, 021001 (2017).
[15] M. Born and K. Huang, *Dynamical Theory of Crystal Lattices* (Oxford University Press, Oxford, 1954).
[16] G. D. Watkins, in *Advanced in Solid State Physics* (Springer, Berlin), Vol. 24, p. 163.
[17] N. Troullier and J. L. Martins, Phys. Rev. B **43**, 1993 (1991).
[18] D. M. Ceperley and B. J. Alder, Phys. Rev. Lett. **45**, 566 (1980).
[19] J. M. Soler, E. Artacho, J. D. Gale, A. Garcia, J. Junquera, P. Ordejon, and D. Sanchez-Portal, J. Phys.: Condens. Matter **14**, 2745 (2002).
[20] H. Jonsson, G. Mills, and K. W. Jacobsen, in *Classical and Quantum Dynamics in Condensed Phase Simulations* (World Scientific, Singapore, 1998), p. 385.
[21] S. R. Bahn and K. W. Jacobsen, Comput. Sci. Eng. **4**, 56 (2002).
[22] E. Runge and E. K. U. Gross, Phys. Rev. Lett. **52**, 997 (1984).
[23] S. Meng and E. Kaxiras, J. Chem. Phys. **129**, 054110 (2008).
[24] O. Sugino and Y. Miyamoto, Phys. Rev. B **59**, 2579 (1999).
[25] R. O. Jones and O. Gunnarsson, Rev. Mod. Phys. **61**, 689 (1989).
[26] Y. Miyamoto, A. Rubio, and D. Tomanek, Phys. Rev. Lett. **97**, 126104 (2006).
[27] T. Frigge, B. Hafke, T. Witte, B. Krenzer, C. Streubuhr, A. Samad Syed, V. Miksic Trontl, I. Avigo, P. Zhou, M. Ligges *et al.*., Nature (London) **544**, 207 (2017).
[28] D. J. Chadi and K. J. Chang, Phys. Rev. Lett. **61**, 873 (1988).
[29] D. J. Chadi and K. J. Chang, Phys. Rev. B **39**, 10063 (1989).
[30] S. B. Zhang and D. J. Chadi, Phys. Rev. B **42**, 7174 (1990).
[31] P. M. Mooney, J. Appl. Phys. **67**, R1 (1990).

[32] M. Mizuta, M. Tachikawa, H. Kukimoto, and S. Minomura, Jap. J. Appl. Phys. **24**, L143 (1985).

[33] D. V. Lang and R. A. Logan, Phys. Rev. Lett. **39**, 635 (1977).

[34] D. V. Lang, R. A. Logan, and M. Jaros, Phys. Rev. B **19**, 1015 (1979).

[35] C. H. Park and D. J. Chadi, Phys. Rev. Lett. **75**, 1134 (1995).

[36] C. H. Park, S. B. Zhang, and S.-H. Wei, Phys. Rev. B **66**, 073202 (2002).

[37] M. D. McCluskey and E. E. Haller, *Dopants and Defects in Semiconductors* (CRC Press, Boca Raton, FL, 2012).

[38] K. Kunc and R. M. Martin, Phys. Rev. Lett. **48**, 406 (1982).

[39] J. Bang, Y. Y. Sun, X.-Q. Liu, F. Gao, and S. B. Zhang, Phys. Rev. Lett. **117**, 126402 (2016).

[40] D. Han, J. Bang, W. Xie, V. Meunier, and S. B. Zhang, J. Phys. Chem. Lett. **7**, 3548 (2016).

[41] J. Bang, Z. Wang, F. Gao, S. Meng, and S. B. Zhang, Phys. Rev. B **87**, 205206 (2013).

[42] P. Lopez-Tarifa, M.-A. Herve du Penhoat, R. Vuilleumier, M.-P. Gaigeot, I. Tavernelli, A. Le Padellec, J.-P. Champeaux, M. Alcami, P. Moretto-Capelle, F. Martín, and M.-F. Politis, Phys. Rev. Lett. **107**, 023202 (2011).

[43] J. Heyd, G. E. Scuseria, and M. Ernzerhof, J. Chem. Phys. **118**, 8207 (2003).

[44] G. Kresse and J. Furthmuller, Comput. Mater. Sci. **6**, 15 (1996).

[45] P. E. Blochl, Phys. Rev. B **50**, 17953 (1994).

[46] H.-P. Komsa and A. Pasquarello, J. Phys.: Condens. Matter **24**, 045801 (2012).

[47] S. K. Sundaram and E. Mazur, Nat. Mater. **1**, 217 (2002).

[48] J. Bang, S. Meng, Y.-Y. Sun, D. West, Z. Wang, F. Gao, and S. B. Zhang, Proc. Natl. Acad. Sci. USA **110**, 908 (2013).

[49] M. A. Reshchikov, A. J. Olsen, M. F. Bishop, and T. McMullen, Phys. Rev. B **88**, 075204 (2013).

[50] S. Jursenas, S. Miasojedovas, G. Kurilcik, A. Zukauskas, and P. R. Hageman, Appl. Phys. Lett. **83**, 66 (2003).

[51] M. Zhang, P. Bhattacharya, J. Singh, and J. Hinckley, Appl. Phys. Lett. **95**, 201108 (2009).

[52] M. Meneghini, N. Trivellin, G. Meneghesso, and E. Zanoni, J. Appl. Phys. **106**, 114508 (2009).

[53] Y. C. Shen, G. O. Mueller, S. Watanabe, N. F. Gardner, A. Munkholm, and M. R. Krames, Appl. Phys. Lett. **91**, 141101 (2007).

[54] A. Alkauskas, C. E. Dreyer, J. L. Lyons, and C. G. Van de Walle, Phys. Rev. B **93**, 201304(R) (2016).

[55] L. Gordon, J. L. Lyons, A. Janotti, and C. G. Van de Walle, Phys. Rev. B **89**, 085204 (2014).

[56] J. Bang, Y. Y. Sun, J.-H. Song, and S. B. Zhang, Sci. Rep. **6**, 24404 (2016).

[57] K. Momma and F. Izumi, J. Appl. Cryst. **44**, 1272 (2011).